Temporal-spatial variations, source apportionment, and ecological risk of trace elements in sediments of water-level-fluctuation zone in the Three Gorges Reservoir, China

Siyuan Zhang [1,2,3], Weiru Wang [1,2,3], Fengwen Wang [1,2,3,*], Daijun Zhang [2,3], Neil L. Rose [4,*]

[1] Key Laboratory of the Three Gorges Reservoir Region' s Eco-Environment, Ministry of Education, Chongqing University, Chongqing 400030, China

[2] State Key Laboratory of Coal Mine Disaster Dynamics and Control, Chongqing University, Chongqing 400030, China

[3] Department of Environmental Science, College of Environment and Ecology, Chongqing University, Chongqing 400030, China

[4] Environmental Change Research Centre, University College London, Gower Street, London WC1E 6BT, United Kingdom

[*] Corresponding author.

E-mail address:

Wang FengWen

fengwenwang@cqu.edu.cn

Rose Neil L.

n.rose@ucl.ac.uk

Abstract

The Three Gorges Reservoir (TGR) plays a crucial role providing electricity for mega-cities across China. However, since the impoundment was completed in 2006, attention

to environmental concerns has also been intensive. In order to determine the distribution, sources and pollution status of trace elements in the water fluctuation zone of the TGR following ten years of repeated "submergence" and "exposure", we systematically collected 16 paired surface sediment samples (n=32) covering the entire main body of the TGR in March 2018 (following six months of submergence) and September 2018 (after six months of exposure), and quantitatively analyzed 13 elements (e.g., Mn, Fe, V, Cr, Ni, Cu, Zn, As, Sr, Y, Zr, Ba and Pb) using X-ray fluorescence spectrophotometry (XRF). The results showed that, except for Sr, concentrations of trace metals following submergence were generally higher than those after exposure, due to the less settling of suspended solids at the faster flow velocity during the drawdown period. Assessment using enrichment factors (EFs) and a geo-accumulation index (I_{geo}) both characterized a relatively serious anthropogenic pollution status of metals in the upper reaches of the TGR with respect to the middle-lower reaches. Source apportionment by positive matrix factorization (PMF) analysis indicated that agricultural activities (24.8% and 24.3%, respectively) and industrial emissions (24.5% and 22.9%, respectively) were the two major sources in these two periods, followed by natural sources, domestic sewage and ore mining. Ecological risk assessment showed that the metalloid arsenic (As) could be the main potential issue of risk to aquatic organisms and human health. A new source-specific risk assessment method (pRI) combined with PMF revealed that agricultural activities could be the major source of potential ecological risk and should be prioritized as the focus of metal/metalloid risk management in the TGR.

Keywords impoundment; trace elements; sources apportionment; ecological risk;

sediments; water level fluctuation zone; Three Gorges Reservoir

Introduction

As one of the largest water storage projects in the world, the Three Gorges Reservoir (TGR) has multiple functions including flood control and power generation, thereby enhancing and altering water resource utilization of the Yangtze River (Dai et al. 2018). The water level of TGR varies through an annual impoundment and release cycle with water levels rising to 175 m in the submergence period (October to April) and falling back to 145 m in the exposure period (May to September). This creates a substantial water-level-fluctuation zone (WLFZ) between Chongqing Municipality and Hubei province with an area of ~ 350 km^2 (Bao et al. 2015). Through changing flow velocities and sediment deposition of TGR, there is a significant impact on the environment of WLFZ. Sources of contamination to this zone, including domestic sewage, ore mining and fertilizer and pesticide applications in riparian regions along the TGR have been recognized (Sun et al. 2013; Zhu et al. 2019). Specifically, the upper section is located in Chongqing city, which is strongly influenced by contaminants discharged from anthropogenic activities such as residential life, shipping and industry (Deyerling et al., 2014; Gao et al., 2016). Industrial parks are intensively distributed in the middle section, where industrial wastewater and exhaust gas flow into nearby tributaries and migrate to the mainstream (Tang et al., 2017). In the downstream with developed agriculture and animal husbandry, chemical fertilizers and pesticides have a great impact on the pollution of WLFZ. Besides, the parent material in this area is mainly limestone, making the trace elements have a relatively high natural background

value with geological conditions (Li et al., 2019; Zhao et al., 2020).

Metals and metalloids such as Cr, Cu, Zn, As and Pb (hereafter trace elements/ metals) have aroused attention within the environment on account of their toxicity and bio-accumulation, which have been a focus of concern in the TGR (Sang et al. 2019; Yan et al. 2020). Recently, Zhao et al. (2020) investigated As, Cr, Cd, Pb, Cu and Zn in sediments during 2015 to 2016, finding a higher health risk to humans at low water level compared with high water level; while Gao et al. (2019a) calculated that between 8.5% and 25.5% of trace metals in sediments of TGR were of anthropogenic origin between 2015 and 2017 by establishing a regional geochemical baseline. Ye et al. (2011) assessed the metal pollution status of sediments in the WLFZ between 2008 and 2009, revealing that Hg, Cd, and Pb were the primary pollutants during submergence, while during exposure, it was As and Cd. These metals were found to have entered the TGR via municipal sewage, industrial wastewater and atmospheric deposition, where they were adsorbed onto clay particles and complexed with organics or oxidized, before being deposited in sediments (Chien et al. 2019). In view of the importance of sediment environmental quality in TGR to the health of both humans and aquatic organisms, temporal-spatial distribution, source identification and ecological risk of metals have all been investigated (Bing et al. 2019). However, most of these studies have only been undertaken on tributaries of the Yangtze River or in local areas of the main body of the TGR, and /or involved only a few metals. Compared with the tributaries, the distribution of sediments along the main body of the TGR is more susceptible to hydrodynamic conditions, more intense human activities and inputs from direct

89 deposition. Therefore, a study on metal pollution in WLFZ of the whole TGR area,
90 would provide valuable data on their abundance, distribution and source variation after
91 ten years of impoundment.

92 Methods including principal component analysis/multiple linear regression
93 (PCA/MLR) and factor analysis (FA) have been used to analyze the sources of metals
94 in TGR (Gao et al. 2019b; Wang et al. 2017b). Isotopic labeling has also been used to
95 distinguish natural and anthropogenic sources of Pb and Hg (Liu et al. 2018). However,
96 to date, there have been no reports on source analysis of trace metal pollution in the
97 TGR using positive matrix factorization (PMF). As a receptor model, the source profiles
98 and contributions obtained from PMF have explanatory and reliable statistical
99 significance (Sun et al. 2020). A combination of source analysis methods for metals in
100 the sediments of the TGR under the cyclical changes of high and low water levels would
101 therefore provide improved information on sources affecting the whole reservoir. In this
102 study, thirteen trace metals (Mn, Fe, V, Cr, Ni, Cu, Zn, As, Sr, Y, Zr, Ba and Pb) were
103 analyzed in 16 paired surface sediment samples (n=32) across the WLFZ of the entire
104 TGR. These samples were collected in March 2018 (following six months of
105 submergence) and September 2018 (after six months of exposure). The major purpose
106 of this study was to 1) identify the different sources of trace metals in the WLFZ using
107 a combination of PCA-MLR and PMF; 2) assess the ecological risk of these trace
108 metals using different methods, thereby providing scientific datasets for environmental
109 management of TGR.

110 ## Materials and methods

Study area and sample collection

The Three Gorges Reservoir zone (106°50'~111°50' E, 29°16'~31°25' N) is located at the tail of the upper reaches of the Yangtze River, between the Zhutuo Hydrographic Station in Chongqing and the Three Gorges Dam (TGD) in Yichang, Hubei Province. Its storage capacity and flood control capacity are 39.3 km^3 and 22.1 km^3, respectively (Tang et al. 2016). The total length of the reservoir is 665 km, and the total submerged surface area is 1084 km^2 (Ye et al. 2019). This region is dominated by mountains (74%) and hills (22%), and belongs to the subtropical humid climate, with annual temperature of 14.9-18.5°C and annual precipitation of 1100-1400 mm (Li et al. 2019). The WLFZ accounts for about 32% of the total area of the TGR.

In this study, sampling was undertaken in March 2018 and September 2018, when the water level dropped from 175m to 163m and rose from 145m to 163m, respectively. In each of these two periods, 16 paired surface sediment samples (n=32, 0-5cm) were collected using a stainless-steel sampler (Peterson, 5 cm diameter and 30 cm length) along the TGR. The sampling sites were selected based on the geographical and hydrological characteristics of the WLFZ from upstream to downstream in the TGR and included Jiangjin (JJ), Xipeng (XP), Beibei (BB), Tongjiaxi (TJX), Chaotianmen (CTM), Jiguanshi (JGS), Tangjiatuo (TJT), Yuzhui (YZ), Changshou (CS), Fuling (FL), Fengdu(FD), Zhongxian (ZX), Wanzhou (WZ), Yunyang (YY), Wushan (WS) and Zigui (ZG) and as shown in Fig. 1 (Ye et al. 2011; Zhao et al. 2020). All sampling sites were away from traffic, industrial parks, sewage outlets and agricultural pollution to avoid direct human influence on heavy metal pollution. At each site, five sampling plots

(2 m ×2 m) were randomly selected in a 200 m^2 area. Then, five surface sediment samples were pooled to provide a composite sample for each plot. All samples were stored dark, in sealed bags and shipped to the laboratory at 4 °C for further analysis.

Chemical analysis

Plant residue and debris greater than 2 mm were removed by sieving the freeze-dried samples in the laboratory. After being ground into homogenous particles in an agate mortar, the samples were screened through a 100-mesh nylon screen and transferred to polythene (PE) bags (Bing et al. 2019). Two grams (accurate to 0.0001g) of the ground samples were weighed into nylon pots with a Mylar film base and compressed. The concentration of elements (e.g., Fe, Mn, V, Cr, Ni, Cu, Zn, As, Sr, Y, Zr, Ba, Pb and Ti) were measured by X-ray fluorescence spectrophotometry (Rigaku NEX CG EDXRF), a well-established method for the determination of commonly heavy metals in solid samples such as soil and sediment (Rose et al. 2020; Cao et al. 2021; Zupancic et al. 2021). It has the advantage of non-destructive, making the same sample can be repeatedly measured with good reproducibility; In addition, the sample does not need too complicated pretreatment, reducing the influence of human factors (Masri et al. 2021). To verify the method accuracy, a certified reference sediment sample of similar mass was measured in each analytical run (Canadian Certified Reference Materials Project; LKSD-2), with mean recovery rates ranging from 96.6% (Ba) to 114.4% (Mn). For the target elements, the relative standard deviation was less than 12%. To reconfirm the quality analysis, a portion of the soil samples (n=11) were subjected to a second round of XRF analysis, which showed a high correlation (r^2>0.99).

After every 10 samples, the blank samples were measured to check for instrument background and possible contamination. All blank samples were below the limit of detection (LOD). The LODs for Fe, Mn, V, Cr, Ni, Cu, Zn, As, Sr, Y, Zr, Ba, Pb and Ti were 6.5, 6.3, 14.8, 4.8, 1.5, 1.9, 0.9, 1.2, 1.1, 0.9, 1.3, 73.0, 1.2 and 15.3 $mg \cdot kg^{-1}$, respectively.

Analysis of physicochemical properties

Physical and chemical properties of the sediments were determined by national standard methods as have been shown in Han et al. (2021). Sediment pH was determined using a pH S-2F digital acidity meter (Leici, Shanghai, China) with a soil/water ratio of 1:5 after being fully shaken. Sediment organic matter (OM) was measured by loss-on-ignition at 550 °C (LOI550) for 3 h (Fu et al., 2020). After acidifying soil samples with excessive hydrochloric acid, total organic carbon (TOC) was determined by total carbon analyzer (TOC-L, Shimadzu, Japan) under the combustion catalytic oxidation method at 680 °C, which was obtained by subtracting inorganic carbon (IC) from total carbon (TC) (Gao et al., 2019). All samples were analyzed in triplicate, and the relative standard deviation was less than 5%. After the sediment samples were screened through a 2mm sieve, the grain-size distribution of the sediments (clay: < 4 μm; silt: 4~63 μm; sand: 63~2000 μm.) (Zhu., et al., 2019) was measured by a dynamic image analyzer (QICPIC/L02-OM, Sympatec, Germany) following ISO 13322-1 and ISO 13322-2. All samples were analyzed in triplicate with the relative standard deviation of particle size distribution less than 3% and median grain size less than 2%.

Data analysis

PCA-MLR

PCA-MLR is a multivariate analysis method that extracts a factor load matrix F (to identify pollution sources) and a factor score matrix G (to calculate source contribution rate) of samples based on a least-squares method. Prior to multivariate analysis, data were standardized to minimize the impact of differences in measurement units (Johnson et al. 2002). Kaiser-Meyer-Olkin (KMO) and Bartlett's sphericity test were applied to examine the suitability of the data for PCA (Helena et al. 2000).

Positive matrix factorization (PMF)

As a receptor model, PMF has been widely used to identify the sources of anthropogenic pollutants in different environmental media (Vu et al. 2017; Niu et al. 2020). The basic principle of PMF is to decompose the original matrix (**X**) into two factor matrices (source composition matrices **G** and source factor matrices **F**) and a residual matrix (**E**), which can be described as follows (eq 1):

$$X_{ij}=\sum_{k=1}^{p} G_{ik}F_{kj}+E_{ij} \quad (1)$$

where X_{ij} refers to the measured content of the i^{th} element in the j^{th} sample; G_{ik} refers to the content of the i^{th} element in the source factor k; F_{kj} refers to the contribution of source factor k to the j^{th} sample; E_{ij} refers to the residual for the corresponding species/sample.

The optimal matrices **G** and **F** are obtained by means of iterative computation using a weighted least square method and continuous decomposition of the acceptor matrix, so that the objective function Q reaches the minimum value. The calculation of

Q is as follows (eq 2):

$$Q=\sum_{i=1}^{n}\sum_{j=1}^{m}\left(\frac{E_{ij}}{U_{ij}}\right)^2 \quad (2)$$

where U_{ij} refers to the uncertainty of the i^{th} element in the j^{th} sample. In this study, the concentrations of metals were all above the method detection limit (MDL), so the uncertainty value is calculated as (eq 3):

$$U_{ij}=\sqrt{(\delta\times C)^2+(0.5\times MDL)^2} \quad (3)$$

where δ is the analytical precision and C is the measured concentration. In this study, the signal-to-noise ratio (SNR) of all elements exceeded 6.0, meeting the requirements of model calculation, and the "robust" mode was adopted to reduce the influence of possible outliers on the PMF solution (Chen et al. 2016). In order to determine the best solution, the model was run for 20 iterations and the initial points with different factor numbers (3~7) were randomly selected (Wang et al. 2015). By comparing the Q value, residual analysis and correlation coefficients between observed and predicted concentrations, we determined an optimal factor number of five, which best explains the information contained in the original data and best meets the needs of the source analysis.

Source-specific analysis of potential ecological risk

The potential ecological risk index (RI) could be used to reflect the potential harm caused by metals to an ecosystem (Hakanson 1980; Bing et al. 2019). It takes into account the concentrations of different metals, their ecological and toxicological effects and biological sensitivity. Details of this method can be found in Text S3. Based on this, in order to assess the contribution of each source to potential ecological risk, a new risk

assessment method combining RI and PMF was adopted in this study. The source-specific risk can be expressed as follows (eq 4 and eq 5):

$$E^{i}_{r(p)}=T_i\times\left(C_{i(p)}/S_i\right) \quad (4)$$

$$pRI=\sum E^{i}_{r(p)} \quad (5)$$

where $E^{i}_{r(p)}$ refers to the potential ecological risk coefficient of the metal *i* in the source factor *p*; $C_{i(p)}$ is the concentration of the metal *i* contributed by factor *p*; S_i is the background values of the metal *i* and shown in Table 2; T_i is the toxic response coefficient of metal *i*, and the T_i value of each element is: As = 10 > Ni = Cu = Pb = 5 > V = Cr = 2 > Mn = Zn = 1 (Hakanson 1980; Fan et al. 2016). pRI is the integrated source-specific risk from factor *p*. Considering that the concentrations of each element were distributed among the 5 factors through PMF source apportionment, the classification of pRI was calculated according to RI. The result of pRI can be classified into five levels: low risk (pRI < 10), moderate risk (10 < pRI < 20), considerable risk (20 < pRI < 40) and high risk (pRI ≥ 40).

Statistical analysis

Paired-samples T test was used to compare the temporal distribution variation of the metals. Pearson correlation analysis was performed to assess the relationships different among metals and soil properties in the samples. All statistical analyses in this study were performed using the software packages SPSS 21.0 and Origin Lab 2018.

Results and discussion

Concentrations and composition of trace metals

The trace metal data for each sample are summarized in Tables S2. Average

243 concentrations for the 13 trace metals (in $mg \cdot kg^{-1}$) are presented in Table 2. The
244 concentrations for the whole TGR, after periods of both submergence and exposure
245 were in the order: Fe > Mn > Zr > Ba > Sr > Zn > V > Cr > Pb > Cu > Y > Ni > As.
246 Overall, the average concentrations of metals after submergence were higher than those
247 before submergence. Only Sr was an exception, with its concentrations of 165.8 $mg \cdot kg^{-1}$
248 and 170.3 $mg \cdot kg^{-1}$, respectively. For Ba, the concentration before submergence was
249 lower than the background value for Chinese soils suggested by Wei et al. (1991); while,
250 for Ni, V and Cr, concentrations before submergence were slightly lower than the soil
251 background values for the TGR area suggested by Tang et al. (2008). By contrast, Zn
252 and Zr concentrations for the two periods were approximately two times higher than
253 the soil background values. Compared with metals data from previous reports for
254 sediments in TGR, the mean concentrations of Mn and Fe in this study (838.9 and
255 37262.6 $mg \cdot kg^{-1}$, respectively) were higher than those measured in 2009 (390 and
256 24205 $mg \cdot kg^{-1}$ respectively) (Ye et al. 2013), while compared with Mn and Cu from
257 2017 (763.6 and 34.6 $mg \cdot kg^{-1}$, respectively) (Xiong et al. 2020), these two metals did
258 not show significant difference. These data therefore suggest that metal concentrations
259 have generally increased over the past decade but that the rate of this increase has
260 slowed down in recent years. As suggested by Lindstrom (2001) and Zhang et al. (2020),
261 this increase in concentrations may be caused by the intensification of anthropogenic
262 activities, such as, industrial wastewater discharge and fertilizer usage along the TGR.
263 Considering these high concentrations and their potential effects on biota, it is
264 reasonable to suggest that the fate and cumulative effects of metals in the TGR deserve

265 further study.

266 Concentrations of trace metals from some other reservoirs of the world are also
267 shown in Table 2. Compared with reservoirs and dams globally, Mn, Fe, Cr, Cu, Ni, Zn
268 and Pb in the TGR are in the mid- to high level. Taking Pb as an example, the mean
269 concentration was 45.0 $mg \cdot kg^{-1}$ and 36.2 $mg \cdot kg^{-1}$ following submergence and exposure,
270 respectively, which was lower than that in Manwan Dam, China and Reservoir
271 Klingenberg, Germany (59.6 and 134 $mg \cdot kg^{-1}$, respectively) (Hahn et al. 2019; Li et al.
272 2019), but higher than El Guájaro Reservoir, Colombia and Sulejów Reservoir, Poland
273 (5.5 and 13.6 $mg \cdot kg^{-1}$, respectively) (Aleksandra et al. 2020; Ana et al. 2018). With a
274 mean of 77.9 and 67.2 $mg \cdot kg^{-1}$ following submergence and exposure in the TGR,
275 respectively, the concentrations of Cr were much higher than that in Aswan High Dam,
276 South Africa and Hoedong Reservoir, Korea (11.8 and 28.7 $mg \cdot kg^{-1}$, respectively)
277 (Farhat et al. 2018; Lee et al. 2017), but lower than that in Insukamini Reservoir,
278 Zimbabwe and the Keban Dam Reservoir, Turkey (Trevor et al. 2019; Varol 2020).
279 Furthermore, the remarkably high concentrations of Mn and Fe in TGR, were more than
280 10 times higher than those in Bontanga Reservoir, Ghana (11.7 and 262.8 $mg \cdot kg^{-1}$,
281 respectively) (Asare et al. 2018).

282 **Temporal-spatial variation of trace metals**

283 The physical and chemical parameters of sediments are summarized in Table 1. In
284 these two periods, the sediments in the WLFZ were weakly alkaline, with a pH range
285 of 7.3-7.9. This could relate to the purplish red soil evolved from the widely distributed
286 sandstone and shale in the upper-middle section, and the carbonate rock composed of

287 limestone and dolomite near the dam area (Bao et al., 2015). The exposed period had a
288 relatively higher content of OM (36.4 $mg \cdot g^{-1}$) with respect to the submergence period
289 (35.3 $mg \cdot g^{-1}$). In summer, abundant terrestrial vegetation and active microorganisms
290 are more suitable for the accumulation of OM (Kallenbach et al., 2016). However, the
291 TOC was higher after submergence, which was related to the strong reduction condition
292 during the water impoundment period (Han et al., 2021). In general, the content of sand
293 and silt at each site in the submergence period was higher than that in the exposure
294 period (Table 1). During submergence, the water flow becomes slow and the water
295 erosion effect is weakened, favoring to the settlement of fine particles (Zhu et al. 2019).
296 Sediment particle sizes, TOC and OM had no significant correlation with metal
297 concentrations, indicating that they hardly have effect on the spatial distribution.

298 Fig. 2 shows the spatial distribution of trace metals at the 16 sites for the two
299 sampling periods. The concentrations of metals upstream (Chongqing City–Fuling) are
300 generally higher than middle (Fuling-Wanzhou) and downstream (Wushan-Zigui),
301 possibly owing to intensive industrial and agricultural activities and shipping
302 transportation in the upstream region (Tang et al. 2014). However, a few metals (e.g.,
303 Cr, Ni, Sr and Ba) in the midstream and downstream areas were still relatively high and
304 did not obviously show this spatial trend. These results could be influenced by the
305 natural weathering of soil material as suggested by Ye et al. (2011). Following the
306 submerged period, the highest concentrations of most metals existed near the urban area
307 of Chongqing, with Fe, V, Cr, Ni, Cu, Zn, As, Y and Pb concentrations at YZ, reaching
308 48900, 105, 105, 35.7, 68.9, 322, 15.2, 38.3 and 79.1 $mg \cdot kg^{-1}$, respectively; while

309 highest Zr and Ba, concentrations were at TJX and CTM (668 and 572 $mg \cdot kg^{-1}$,
310 respectively). The exceptions were Mn and Sr, for which the highest concentrations
311 occurred at CS and WZ, 1380 and 199 $mg \cdot kg^{-1}$, respectively. The lowest concentrations
312 of most metals were located in the middle and lower reaches, with the exceptions of Zr
313 and Ba. The lowest concentrations of Mn, Fe, V, Ni, Zn, As, Y and Pb were all at WS,
314 where they were 442, 31000, 61, 24.6, 65.8, 5.98, 27.3 and 24.3 $mg \cdot kg^{-1}$, respectively.
315 Located in the border zone between Chongqing and Hubei province, WS is
316 underdeveloped with respect to industry and agriculture, resulting in a low level of
317 release for these metals (Li et al. 2017).

318 The exposed period showed a number of differences in spatial distributions.
319 Concentrations of Mn, Fe, V, Ni, Y and Ba were highest at XP (1270, 43800, 93, 34.7,
320 34.6 and 584 $mg \cdot kg^{-1}$ respectively); while Zn and As concentrations were highest at
321 JGS and TJX (186 and 12.1 $mg \cdot kg^{-1}$, respectively). With regard to the other five metals,
322 the highest concentrations were all in the middle reaches with Cr, Cu and Pb reaching
323 highest concentrations at ZX (82, 51.5 and 58.4 $mg \cdot kg^{-1}$, respectively). Extensive use
324 of chemical fertilizers and pesticides in agricultural production in this area could result
325 in this distribution (Ye et al. 2011).

326 A comparison of the 13 metals, TOC and OM between submerged and exposed
327 periods are presented in Fig. S1. Suspended matter in the water column usually settles
328 naturally to cover the surface of the submerged zone to form sediments. However,
329 during the water drawdown period, metals may be released more quickly into the water
330 as a result of faster flow velocity, resulting in reduced deposition of suspended solids

and reduced metal content. Using a paired-sample T-test, the content of Fe and Y decreased very significantly (p<0.01), while Cr and Ni decreased significantly (p<0.05). With the rise in water level during the flood period, the WLFZ in the TGR was gradually submerged. As a result, transport and exchange of material between the banks and upper areas of the catchment is frequent, so that allochthonous material may be transported into the TGR system. These imported sediments include metals from point source emissions in urban areas and non-point source emissions from agriculture (Bing et al. 2019), inevitably affecting the environmental quality of sediments deposited during the submerged period.

Assessment of metal contamination

Enrichment factor (EF) is a parameter used to evaluate the influence of human activities on metals in soil and sediment (Barbieri et al. 2016). EF calculation are summarized in Text S1. Elements with stable geochemical properties have been widely used as reference elements, such as Al, Fe, Li, Sc, Ti and Zr (Loska et al. 1997; Reimann et al. 2005). Ti was selected for this study due to its reduced mobility in soils and sediments and weak differentiation during weathering and soil formation (Churchman et al. 2012). Local background values for the metals in this study are shown in Table 2 following Wei et al. (1991) and Tang et al. (2008).

Fig. 3a compares the EFs of 13 metals between the submerged and exposed periods. EFs for each metal and associated statistical characteristics are also summarized in Tables S3 and S4. According to Sutherland (2000), there are five levels of EFs ranging from <2 indicating natural sources and minimal pollution, through to EFs >40

353 indicative of extreme pollution. In this study, the EFs of Fe, V, Cr, Ni, Ba and Y in all
354 samples, and Sr in the submerged period were less than 1.5, indicating that they were
355 from natural sources, such as weathering of crustal rocks (Zhang et al. 2002). For
356 samples taken following submergence, metals at TJT, YZ and CS had higher EFs than
357 other sites. The average EFs of Zn and Zr were higher than 1.5, indicating some
358 anthropogenic activity. For Zn, the sites from TJT to CS were moderately enriched
359 (EF>2), while 62.5% of the sites were slightly enriched (1<EF<2). For Zr, TJT and ZG
360 were moderately enriched (EF>2), while the rest of sites were slightly enriched
361 (1<EF<2). EF>1.5 were also observed in the upper reaches for Mn, Cu, As and Pb. In
362 particular, Mn at CS and Pb at TJT showed moderate enrichment (EF>2). Following
363 the period of exposure, the metals at XP, BB, JGS, TJT, YY and WS showed relatively
364 high enrichment with respect to other sites. The average EFs of most metals were less
365 than 1.5 except for Zr. EFs of Zr in BB, YY and JGS to FL were moderately enriched
366 (EF>2), while the other sites were slightly enriched (1<EF<2). In contrast to the
367 submerged samples, As, Sr and Pb at some sites of the middle and lower reaches (e.g.,
368 ZX, YY, WS and ZG) following exposure were affected by human activities, with
369 EF>1.5. In general, the order of average EFs following submergence was Zr ≈ Zn >>
370 Pb ≈ Mn ≈ As ≈ Cu ≈ Y >> Fe ≈ Sr >> V ≈ Ni ≈ Ba ≈ Cr; while after exposure, the
371 order was Zr >> Zn ≈ Mn ≈ Pb ≈ As ≈ Y ≈ Sr ≈ Cu ≈ Fe >> Ba ≈ Ni ≈ V > Cr.

372 Aside from EFs, the geo-accumulation index (I_{geo}), has also been widely used to
373 assess the extent of metal pollution in soils and sediments caused by human activities
374 (Muller 1969). Calculation of I_{geo} is summarized in Text S1. The associated statistical

characteristics are summarized in Tables S5 and S6. Fig. 3b compares the I_{geo} of 13 metals between the submerged and exposed periods. According to Muller (1969), there are seven levels of I_{geo} ranging from uncontaminated (≤ 0) to extremely contaminated (> 5). The I_{geo} of V, Cr, Ni and Ba in all samples were < 0, while for Mn, Fe, Cu, As, Sr and Y, the $I_{geo} < 1$. With a mean of 0.8 and 0.7, the I_{geo} of Zr was the highest of all metals, except for TJT, YZ where Zn was highest, XP (Pb) and CS (Mn) during submergence, and for XP (Mn) and WS (Sr) during exposure. For Zn, 62.5% of the sampling sites for both submerged and exposed periods were slightly contaminated; while moderate contamination was only observed in TJT and YZ following submergence. For Pb, most of the sampling sites were either uncontaminated or slightly contaminated, with the exception of YZ where moderate contamination was observed during the submerged period.

According to the EFs and I_{geo} calculated above, most HMs had a similar degree of enrichment although slight differences in the sequencing of some metals may be observed. Reimann et al. (2000) reported that study elements and reference elements should have a similar geochemical migration and cycling characteristics during soil formation. However, the geochemical characteristics of some metals in this study may be different from the selected reference element Ti and this would slightly affect the calculated EFs. Even so, the spatial distribution of the EFs was basically the same as that of I_{geo} (Tables S4 and S6) and both indicated that, except for Zr, contamination in the upper reaches of the TGR is generally more serious than those in the middle and lower reaches.

Source identification of metals using PCA-MLR and PMF

Based on previous studies, it could be found that metals in the sediments of the TGR have combined source characteristics (Gao et al. 2019b; Liu et al. 2018). Different trace metals may come from multiple sources, and source contributions vary over time. In order to identify metal pollution sources and compare the source contribution of the two models, we selected 9 common metals (e.g., Mn, Fe, V, Cr, Ni, Cu, Zn, As and Pb). According to the results of Kaiser-Meyer-Olkin and Bartlett's sphericity test, the correlations between the variables were sufficiently significant for subsequent PCA (Zhou et al. 2007). Three principal components (PCs) were extracted in the PCA, accounting for 90.7% and 87.6% of the total variance during submergence and exposure, respectively. During the submerged period, PC1 had high loadings of Cu, Pb and Zn, accounting for 33.6% of total variables. Pb is widely present in sewage irrigation, whereas Cu and Zn are often applied in aquaculture feed additives and thereby entering sediments through faeces (Kabata-Pendias et al. 1992; Wang et al. 2013). Zn also is widely applied to crops and vegetables as a component of some fungicides (Chen et al. 2016) and has many possible sources including mining, smelting and industrial processing of zinc-bearing ore (Kaya et al. 2020). Therefore, PC1 was identified as multiple sources of agricultural activities and ore mining, such as use of fertilizers, livestock feeding, sewage irrigation and zinc-bearing ore. With high loadings of Mn and As, PC2 contributed 32.2% of total variables. The proven reserves of manganese ore in Chongqing is the second highest nationally, and is mainly used in industries including metallurgy, electronic manufacture and chemical engineering. Ye

et al. (2011) found that As is related to the discharge of domestic sewage. Samples with high concentrations of Mn and As were mainly collected from areas near electronic industries, such as BB and ZX, and therefore PC2 was assigned to industrial emissions and domestic sewage. PC3 had relatively high loads of V, moderate loads of Fe and Ni, contributing 24.9% of the total variables. Fe is the typical element in natural geological environment and mainly come from soil erosion and mineral weathering as well (Matthews et al. 1983). Significantly, the EFs of Fe, V and Ni were lower than 1.5 in all samples (Table S3) and therefore PC3 could be assigned as natural sources.

Following exposure, PC1 accounted for 41.4% of the total variation and had significant loadings from Cu, Pb and Zn. We therefore assign this to the same sources (agricultural activities and ore mining) as for the submerged period. With a contribution of 20.3% of the total variation, PC2 is mainly characterized by As and V. As mainly derives from domestic sewage, and V is widely used in iron and steel industry as an alloying agent as well as present in many oil combustion products (Ali et al. 2020; Han et al. 2020). High concentrations of As and V were mainly in samples collected in sites close to industrial centres, such as YF, CS and JGS. Therefore, PC2 was considered indicative of multiple sources of domestic sewage and industrial emissions. Accounting 25.9% of the total variation, PC3 has high loadings of Cr, moderate loadings of Ni and Fe, with their EFs < 1.5 (Table S3). Thus, PC3 was assigned as natural source.

Multivariate linear regression (MLR) was applied to calculate the contributions of three identified sources of metals based on the PCA factor scores. The source categories and factor scores are shown in Fig. 4a. The formula for source contribution rate were

441 described in Text S2. By contrast, PMF resulted in five source categories as shown in
442 Fig. 4b. The relative contributions from these categories are summarized in Table 3. It
443 could be seen that PMF apportionment can better show the complex pollution in the
444 TGR area. For V, Cr and Ni, industrial emissions and natural sources are major
445 contributors. Cu and Pb primarily come from agricultural activities and industrial
446 emissions, while Zn is mainly derived from ore mining and agricultural activities. After
447 submergence, factor 1 was responsible for 6.3% of the measured metals and has a high
448 loading for Zn (56% of the factor 1 loading) and therefore factor 1 may represent ore
449 mining and processing. Factor 2 contributed 21.7% and had highest loadings from As.
450 Based on PCA identification, factor 2 could be associated with domestic sewage. Factor
451 3 explained 24.5% of the measured metals. Its main loading is Cr and highly weighted
452 on Ni and Cu. As important components of mining, steel and chemical industries, Cr
453 and Ni could enter the TGR through atmospheric deposition and surface runoff (Chen
454 et al. 2016; Zhao et al. 2020). Factor 3 could be regarded as industrial emissions. Factor
455 4 contributed 24.8% of the metals. It was predominantly weighted by Cu and Pb.
456 Sewage and fertilizer applications result in a large number of heavy metals such as Cu
457 and Pb being applied to agricultural soils (Han et al. 2018). Furthermore, Cu is widely
458 used as an insecticide for fruit trees in the form of $CuSO_4$ and as a feed additive to
459 accelerate the growth of livestock (Chen et al. 2016). Thus, factor 4 could be considered
460 as indicative of agricultural activities. Factor 5 accounted for 22.8% of the metals. It
461 was mainly loaded by Fe, V, Cr and Ni. Fe is a relatively abundant in the Earth's crust
462 and it should be noted that the EFs of Fe, V, Cr and Ni were all lower than 1.5 (Table

463 S3). Factor 5 was therefore assigned natural sources.

464 Five similar source categories were also identified for the samples taken following
465 exposure, but the contribution ratios varied for each (Fig. 4b). Therefore, we conclude
466 that agricultural activities (24.8% and 24.3%, respectively) and industrial emissions
467 (24.5% and 22.9%, respectively) were the two major sources in both periods, followed
468 by natural sources (22.8%) after submergence, and ore mining (21.5%) after exposure.
469 Domestic sewage accounted for 21.7% after submergence, but following exposure it
470 was only 14.0%. During the submersion period, metals such as As in domestic sewage
471 are more likely to enter the reservoir and deposit in the sediments due to the lower flow
472 velocity. The source contribution from ore mining and processing varied considerably
473 between the two periods, and also forms part of industrial activities in the region. In
474 this study, ore mining is mainly represented by zinc-bearing ore during the submerged
475 period; but during the exposed period, it could also include iron and manganese ore, as
476 well as arsenic pollution caused by processing and smelting (Barcelos et al. 2020; Fry
477 et al. 2020). These combined contamination pathways therefore need to be taken into
478 account when considering abatement strategies for reducing trace metal pollution in the
479 unique cyclical environment of the WLFZ of the TGR.

480 **Potential ecological risk from metals in the TGR**

481 The E_r^i and RI of the eight metals for the two periods are summarized in Fig. 5
482 and Table S7. Between the two periods, only the E_r^i of Cr and Ni showed a significant
483 difference (p<0.05). Following submergence, the E_r^i of As varied between 10.2 and
484 26.0 through the TGR, with a mean of 17.5; while during exposure, it varied between

9.0 and 20.7, with a mean of 14.7, both characterizing a moderate potential ecological risk. Total RI values varied between 30.3 and 74.7, with a mean of 48.7 following submergence; while after exposure, it ranged from 31.1 and 52.3, with a mean of 41.0. The total RI was significantly higher after submergence than after exposure (p<0.05).

Apart from Cr and Ni, the average E_r^i values of other metals in the two periods were lower than 10, suggesting a low potential ecological risk. However, As showed a high potential risk level at TJX, YZ and CS after submergence and at TJX after exposure, but at other sites there was only a moderate risk except at YY after exposure. A moderate potential ecological risk was identified for Pb at JGS to CS, JJ, XP, BB (the upstream areas) and at JJ, JGS, ZX following submergence and exposure periods, respectively. Moderate ecological risk from Cu was observed at JJ, XP, TJT, YZ and at ZX following submergence and exposure periods, respectively. For the other metals, they pose only a rather low potential risk for both periods. Although Cr (2.0 and 1.7, respectively) and Ni (5.2 and 4.8, respectively) posed a low ecological risk, there is great need to pay attention on their geochemical behavior and ecological risk in sediments due to the reduced sediment load from the upper reaches and the rapid urbanization in the TGR area (Wang et al. 2017a).

A new source-specific ecological risk method (pRI), which is combined with PMF, was used to analyze the risk contributions from different sources, and the results are shown in Fig. 6. Due to the different toxic response coefficients of each toxic element, the concentration proportion of the source may not be consistent with the corresponding risk level. In this study, following submergence, agricultural activities and domestic

sewage contributed the majority risk of metals in surface sediment (31.4% and 24.9%, respectively), and both imposed the moderate ecological risk (15.3 and 12.1, respectively). During the high-water-level period, toxic metals from pesticides and fertilizers application and residual domestic wastes in surrounding areas will be brought into the water environment (Tang et al. 2014). At the same time, low water velocity is not conducive to the diffusion of pollutants, leading to further deterioration of the water environment (Fu et al. 2010). Industrial emissions accounted 20.0% for the total risk, which was close to the moderate ecological risk (pRI = 9.7). Following exposure, all the sources exhibited a relatively low risk (pRI < 10). Nevertheless, industrial emissions and agricultural activities were both close to the moderate source-specific risk (9.3 and 9.0, respectively), and constituted a significant part of the risk to the reservoir. Sources dominated by highly toxic metals (e.g., As and Pb) were likely to pose more ecological risks than those dominated by low toxic heavy metals (e.g., Mn and Zn).

Conclusion

The average concentrations of 13 metals following submergence were generally higher than those after exposure. Based on comparisons with previously study, the concentrations of metals in the WLFZ of TGR have increased over the past decade. The metals in the upper reaches of the TGR was generally higher than those in the middle and lower reaches, but Cr, Ni, Sr and Ba did not show obviously similar spatial variation trend. The average EFs of metals were in the order: Zr ≈ Zn >> Pb ≈ Mn ≈ As ≈ Cu ≈ Y >> Fe ≈ Sr >> V ≈ Ni ≈ Ba ≈ Cr following submergence; while following exposure it was Zr >> Zn ≈ Mn ≈ Pb ≈ As ≈ Y ≈ Sr ≈ Cu ≈ Fe >> Ba ≈ Ni ≈ V > Cr. The I_{geo} also

showed an obvious contamination from Zr. PCA-MLR apportioned three source categories: agricultural activities/ore mining, industrial emissions/ domestic sewage and natural sources, with contributions of 37.8%, 39.3% and 22.9% following submergence and 50.9%, 22.8% and 26.3% after exposure, respectively. PMF identified 5 sources and indicated that the highest contributor for metals was agricultural activities, contributing 24.8% following submergence and 24.3% after exposure. Potential ecological index suggested that trace metals in sediments had a low to moderate potential eco-risk. A new source-specific risk method pRI identified that the major integrated ecological risk was from agricultural activities.

Acknowledgements This work was funded by the National Natural Science Foundation of China (NSFC) (No: 42077319, 41603102); National Key R&D Program of China (No: 2019YFC1805500), Technological Innovation and Application Development Key Projects of Chongqing Municipality, China (No: cstc2019jscx-gksb0241).

Declarations

Ethics approval Not applicable.

Consent to participate Not applicable.

Consent for publication Not applicable.

Author contribution： Fengwen Wang and Daijun Zhang performed the research; Neil L. Rose analyzed data; Siyuan Zhang and Weiru Wang wrote the paper. All the co-authors substantially contributed to commenting and revising it. All authors read and approved the final manuscript.

Conflict of interest The authors declare no competing interest.

Data availability: All data generated or analysed during this study are included in supporting information.

References

Aleksandra Z-S, Ewa I, Marcin J, Aleksander S (2020) Assessment of the Chemical State of Bottom Sediments in the Eutrophied Dam Reservoir in Poland. Int J Env Res Pub He 17 (10): 3424

Ali W, Mao K, Zhang H, Junaid M, Xu N, Rasool A, Feng XB, Yang ZG (2020) Comprehensive review of the basic chemical behaviours, sources, processes, and endpoints of trace element contamination in paddy soil-rice systems in rice-growing countries. J Hazard Mater 397: 122720

Ana CT-E, Eliana M-M, Daniel C-V, Luis CG-M, Franklin T-B (2018) Contamination Level and Spatial Distribution of Heavy Metals in Water and Sediments of El Guájaro Reservoir, Colombia. B Environ Contam Tox 101(1): 61–67

Asare ML, Cobbina SJ, Akpabey FJ, Duwiejuah AB, Abuntori ZN (2018) Heavy Metal Concentration in Water, Sediment and Fish Species in the Bontanga Reservoir, Ghana. Toxicol Environ Health Sci 10(1): 49–58

Bao YH, Gao P, He XB (2015) The water-level fluctuation zone of Three Gorges Reservoir: a unique geomorphological unit. Earth-Sci Rev 150: 14–24

Barbieri M (2016) The Importance of Enrichment Factor (EF) and Geoaccumulation Index (Igeo) to Evaluate the Soil Contamination. Journal of Geology & Geophysics: 5

573 Barcelos DA, Pontes FVM, da Silva FANG, Castro DC, dos Anjos NOA, Castilhos ZC
574 (2020) Gold mining tailing: Environmental availability of metals and human
575 health risk assessment. J Hazard Mater 97: 122721
576 Bing HJ, Wu YH, Zhou J, Sun HY, Wang XX, Zhu H (2019) Spatial variation of heavy
577 metal contamination in the riparian sediments after two-year flow regulation in the
578 Three Gorges Reservoir, China. Sci Total Environ 649: 1004–1016
579 Cao YH, Li XP, He F, Sun XM, Zhang X, Yang T, Dong J, Gao Y, Zhou QS, Shi DQ,
580 Wang JW, Yu HT (2021) Comprehensive screen the lead and other toxic metals in
581 total environment from a coal-gas industrial city (NW, China): Based on integrated
582 source-specific risks and site-specific blood lead levels of 0-6 aged children.
583 Chemosphere 278: 130416
584 Chen HY, Teng YG, Li J, Wu J, Wang JS (2016) Source apportionment of trace metals
585 in river sediments: a comparison of three methods. Environ Pollut 211: 28–37
586 Cheng H, Liang A, Zhi Z (2017) Heavy metals sedimentation risk assessment and
587 sources analysis accompanied by typical rural water level fluctuating zone in the
588 Three Gorges Reservoir Area. Environ Earth Sci 76(12): 418
589 Chien CT, Benahabet T, Torfstein A, Paytan A (2019) Contributions of Atmospheric
590 Deposition to Pb Concentration and Isotopic Composition in Seawater and
591 Particulate Matters in the Gulf of Aqaba, Red Sea. Environ Sci Technol 53(11):
592 6162–6170
593 Churchman GJ, Lowe DJ (2012) Alteration, Formation, and Occurrence of Minerals in
594 Soils. In: Huang, PM, Li Y, Summer ME (Eds.). Handbook of Soil Science, 2nd

595 edition, Vol.1, Properties and Processes, CRC Press (Taylor & Francis), Boca
596 Raton, FL, pp.20.1-20.72
597 Dai L, Zhou JZ, Chen L, Huang KD, Wang QS, Zha G (2018) Flood-risk analysis based
598 on a stochastic differential equation method. J Flood Risk Manag 12(S1): e12515
599 Deyerling D, Wang J, Hu W, Westrich B, Peng C, Bi Y, Henkelmann B, Schramm KW
600 (2014) PAH distribution and mass fluxes in the Three Gorges Reservoir after
601 impoundment of the Three Gorges Dam. Sci Total Environ 491-492: 123-130
602 Fan MY, Yang H, Huang XF, Cao RS, Zhang ZD, Hu JW, Qin FX (2016) Chemical
603 forms and risk assessment of heavy metals in soils around a typical coal-fired
604 power plant located in the mountainous area. China Environ Sci 36(8): 2425–2436
605 (in Chinese)
606 Farhat HI, Aly W (2018) Effect of site on sedimentological characteristics and metal
607 pollution in two semi-enclosed embayments of great freshwater reservoir: Lake
608 Nasser, Egypt. J Afr Earth Sci 141: 194–206
609 Fry KL, Wheeler CA, Gillings MM, Flegal AR, Taylor MP (2020) Anthropogenic
610 contamination of residential environments from smelter As, Cu and Pb emissions:
611 Implications for human health. Environ Pollut 262: 114235
612 Fu BJ, Wu BF, Lu YH, Xu ZH, Cao JH, Niu D, Yang GS, Zhou YM (2010) Three gorges
613 project: efforts and challenges for the environment. Prog Phys Geogr 34: 741–754
614 Fu C, Lan QJ, Wu Y, Yan B, Ping W, Huang L, Yang BR (2020) Influence of Sediment
615 Characteristics on Heavy Metal Fraction Distribution in the Water-Level
616 Fluctuation Zone of the Three Gorges Reservoir Area, China. Water Air Soil Poll

231 (4): 175

Gao J, Sun X, Jiang W, Wei Y, Guo J, Liu Y, Zhang K (2016) Heavy metals in sediments, soils, and aquatic plants from a secondary anabranch of the three gorges reservoir region, China. Environ Sci Pollut Res 23: 10415–10425

Gao L, Gao B, Xu DY, Peng WQ, Lu J (2019) Multiple assessments of trace metals in sediments and their response to the water level fluctuation in the Three Gorges Reservoir, China. Sci Total Environ 648: 197–205

Gao Q, Li Y, Cheng QY, Yu MX, Hu B, Wang ZG, Yu ZQn(2019b) Analysis and assessment of the nutrients, biochemical indexes and heavy metals in the Three Gorges Reservoir, China, from 2008 to 2013. Water Res 92: 262–274

Gao SP, Xu BQ, Wang JB, Cong ZY (2019) Measuring total organic carbon precisely in lake sediment in Tibetan plateau by TOC analyzer. Chinese J Anal Lab 38 (4): 413–416 (in Chinese)

Hahn J, Opp C, Ganzenmuller R, Ewert A, Schneider B, Zitzer N, Laufenberg G (2019) Catchment soils as a factor of trace metal accumulation in sediments of the reservoir Klingenberg (eastern Ore Mountains, Germany). J Environ Sci 86: 1–14

Hakanson L (1980) An ecological risk index for aquatic pollution control, a sedimentological approach. Water Res 14(8): 975–1001

Han XK, Wang FW, Zhang DJ, Feng T, Zhang LL (2021) Nitrate-assisted biodegradation of polycyclic aromatic hydrocarbons (PAHs) in the water-level-fluctuation zone of the three Gorges Reservoir, China: Insights from in situ microbial interaction analyses and a microcosmic experiment. Environ Pollut 268:

115693

Han Y, Zhang SH, Bai R, Zhou H, Su Z, Wu JJ, Wang JL (2020) Effect of nano-vanadium nitride on microstructure and properties of sintered Fe-Cu-based diamond composites. Int J Refract Met H 91: 105256

Han ZX, Wang XQ, Chi QH, Zhang BM, Liu DS, Wu H, Tian M (2018) Occurrence and source identification of heavy metals in the alluvial soils of Pearl River Delta region, south China. China Environ Sci 38(9): 3455–3463 (in Chinese)

Helena B, Pardo R, Vega M, Barrado E, Fernandez JM, Fernandez L (2000) Temporal evolution of groundwater composition in an alluvial aquifer (Pisuerga River, Spain) by principal component analysis. Water Res. 34: 807–816.

Johnson RA, Wichern DW (2002) Applied Multivariate Statistical Analysis, 5th ed. Prentice-Hall NJ

Kabata-Pendias A, Pendias H (1992) Trace Elements in Soils and Plants (2nd Ed.). CRC Press, Boca Raton, FL

Kallenbach CM, Frey SD, Grandy AS (2016) Direct evidence for microbial-derived soil organic matter formation and its ecophysiological controls. Nat Commun 7: 13630

Kaya M, Hussaini S, Kursunoglu S (2020) Critical review on secondary zinc resources and their recycling technologies. Hydrometallurgy 195: 105362

Lee P-K, Kang M-J, Yu S, Ko K-S, Ha K, Shin S-C, Park JH (2017) Enrichment and geochemical mobility of heavy metals in bottom sediment of the Hoedong reservoir, Korea and their source apportionment. Chemosphere 184: 74–85

Li HG, Wang JY, Yang S, Cui J, Liu K, Yuan S, Zhang Y, Zhang S, Cheng M (2017)

661 Reviews on soil heavy metals pollution and its environment risk in the Three
662 Gorges Reservoir Area. Environ Sci Technol 40(S2): 171–178 (in Chinese)
663 Li JL, Bao YH, Wei J, He XB, Tang Q, Nambajimana JD (2019) Fractal characterization
664 of sediment particle size distribution in the water-level fluctuation zone of the
665 Three Gorges Reservoir, China. J Mt Sci 16(9): 2028-2038
666 Li JP, Cheng DM, Zhao AD, Dong SK, You XG (2019) The characteristics and the
667 assessment of heavy metal and nutrient pollution in sediments of cascading
668 hydropower dams in Lancang River. Acta Scien Circum 39(8): 2791–2799 (in
669 Chinese)
670 Li Y, Xu D, Gao L, Gao B (2019) Reviews on soil metal pollution in water-level
671 fluctuation zone of Three Gorges Reservoir area. J China Inst Water Resour
672 Hydropower Res 17: 152–160 (in Chinese)
673 Lindstrom M (2001) Urban land use influences on heavy metal fluxes and surface
674 sediments concentrations of small lakes. Water Air Soil Poll 126(3–4): 363–383
675 Liu JL, Bi XY, Li FL, Wang PC, Wu J (2018) Source discrimination of atmospheric
676 metal deposition by multi-metal isotopes in the Three Gorges Reservoir region,
677 China. Environ Pollut 240: 582–589
678 Liu MX, Yang YY, Yun XY, Zhang MM, Wang J (2015) Concentrations, distribution,
679 sources, and ecological risk assessment of heavy metals in agricultural topsoil of
680 the Three Gorges Dam region, China. Environ Monit Assess 187(3): 147
681 Loska K, Cebula J, Pelczar J, Wiechuła D, Kwapuliński J (1997) Use of enrichment,
682 and contamination factors together with geoaccumulation indexes to evaluate the

683 content of Cd, Cu, and Ni in the Rybnik water reservoir in Poland. Water Air Soil
684 Poll 93(1–4): 347–365
685 Masri S, LeBron AMW, Logue MD, Valencia E, Ruiz A, Reyes A, Wu J (2021) Risk
686 assessment of soil heavy metal contamination at the census tract level in the city
687 of Santa Ana, CA: implications for health and environmental justice. Environ Sci:
688 Processes Impacts 23: 812
689 Matthews WH (1983) Chapter Six - Weathering and Soil Formation. In the Made
690 Simple Series, Geology (Second Edition) 77-82.
691 Muller G (1969) Index of geoaccumulation in sediments of the Rhine River. GeoJournal
692 2(3): 109–118
693 Niu Y, Jiang X, Wang K, Xia JD, Jiao W, Niu Y, Yu H (2020) Meta analysis of heavy
694 metal pollution and sources in surface sediments of Lake Taihu, China. Sci Total
695 Environ 700(15): 134509
696 Reimann C, Caritat PD (2000) Intrinsic flaws of element enrichment factors (EFs) in
697 environmental geochemistry. Environ Sci Technol 34: 5084–5091
698 Reimann C, Caritat PD (2005) Distinguishing between natural and anthropogenic
699 sources for elements in the environment: regional geochemical surveys versus
700 enrichment factors. Sci Total Environ 337(13): 91–107
701 Rose NL, Milner AM, Fitchett JM, Langerman KE, Yang H, Turner SD, Jourdan A-L,
702 Shilland J, Martins CC, de Souza AC, Curtis CJ (2020) Natural archives of long-
703 range transported contamination at the remote lake Letseng-la Letsie, Maloti
704 Mountains, Lesotho. Sci Total Environ: 139642

Sang C, Zheng YY, Zhou Q, Li DP, Liang GD, Gao YW (2019) Effects of water impoundment and water-level manipulation on the bioaccumulation pattern, trophic transfer and health risk of heavy metals in the food web of Three Gorges Reservoir (China). Chemosphere 232: 403–414

Sun CC, Shen ZY, Liu RM, Xiong M, Ma FB, Zhang O, Li YY, Chen L (2013) Historical trend of nitrogen and phosphorus loads from the upper Yangtze River basin and their responses to the Three Gorges Dam. Environ Sci Pollut R 20(12): 8871–8880

Sun X, Wang HQ, Guo ZG, Lu PL, Song FZ, Liu L, Liu JX, Rose NL, Wang FW (2020) Positive matrix factorization on source apportionment for typical pollutants in different environmental media: a review. Environ Sci-Proc Imp 20(2): 239–255

Sutherland RA (2000) Bed sediment-associated trace metals in an urban stream, Oahu, Hawaii. Environ Geol 39: 611–627

Tang J, Zhong YP, Wang L (2008) Background value of soil heavy metal in the Three Gorges Reservoir District. Chinese J Eco-Agr 16(4): 848–852 (in Chinese)

Tang Q, Bao YH, He XB, Fu BJ, Collins AL, Zhang XB (2016) Flow regulation manipulates contemporary seasonal sedimentary dynamics in the reservoir fluctuation zone of the Three Gorges Reservoir, China. Sci Total Environ 548–549: 410–420

Tang Q, Bao YH, He XB, Zhou HD, Cao ZJ, Gao P, Zhong RH, Hu YH, Zhang XB (2014) Sedimentation and associated trace metal enrichment in the riparian zone of the Three Gorges Reservoir, China. Sci Total Environ 479–480: 258–266

727 Tang YM, Junaid M, Niu A, Deng S, Pei DS (2017) Diverse toxicological risks of PAHs
728 in surface water with an impounding level of 175m in the Three Gorges Reservoir
729 Area, China. Sci Total Environ 580: 1085-1096
730 Trevor D, Grace M, Caston M, Bridget P, Tinashe M (2019) Spatial variation of heavy
731 metals and uptake potential by Typha domingensis in a tropical reservoir in the
732 midlands region, Zimbabwe. Environ Sci Pollut R 26(10): 10097–10105
733 Varol M (2020) Environmental, ecological and health risks of trace metals in sediments
734 of a large reservoir on the Euphrates River (Turkey). Environ Res 187: 109664
735 Vu CT, Shern CC, Yeh G, Le VG, Tran HT (2017) Contamination, ecological risk and
736 source apportionment of heavy metals in sediments and water of a contaminated
737 river in Taiwan. Ecol Indic 82: 32-42
738 Wang FW, Lin T, Feng JL, Fu HY, Guo ZG (2015) Source apportionment of polycyclic
739 aromatic hydrocarbons in PM2.5 using positive matrix factorization modeling in
740 Shanghai, China. Environ Sci-Proc Imp 17(1): 197–205
741 Wang H, Dong YH, Yang YY, Toor GS, Zhang XM (2013) Changes in heavy metal
742 contents in animal feeds and manures in an intensive animal production region of
743 China. J Environ Sci 25(12): 2435–2442
744 Wang XX, Bing HJ, Wu YH, Zhou J, Sun HY (2017a) Distribution and potential eco-
745 risk of chromium and nickel in sediments after impoundment of Three Gorges
746 Reservoir, China. Hum Ecol Risk Assess 23(1): 172–185
747 Wang YY, Wen AB, Guo J, Shi ZL, Yan DC (2017b) Spatial distribution, sources and
748 ecological risk assessment of heavy metals in Shenjia River watershed of the Three

749 Gorges Reservoir Area. J Mt Sci-Engl 14(2): 325–335
750 Wei FS, Chen JS, Wu YY (1991) Study on the background value of soil environment
751 in China. Chinese J Environ Sci 12(4): 12–19 (in Chinese)
752 Xiong B, Li RP, Johnson D, Luo YH, Xi Y, Ren D, Huang YP (2020) Spatial
753 distribution, risk assessment, and source identification of heavy metals in water
754 from the Xiangxi River, Three Gorges Reservoir Region, China. Environ
755 Geochem Hlth
756 Yan W, Hamid N, Deng S, Jia PP, Pei DS (2020) Individual and combined toxicogenetic
757 effects of microplastics and heavy metals (Cd, Pb, and Zn) perturb gut microbiota
758 homeostasis and gonadal development in marine medaka (Oryzias melastigma). J
759 Hazard Mater 397: 122795
760 Ye C, Butler OM, Du M, Liu WZ, Zhang QF (2019) Spatio-temporal dynamics, drivers
761 and potential sources of heavy metal pollution in riparian soils along a 600
762 kilometre stream gradient in Central China. Sci Total Environ 651: 1935-1945
763 Ye C, Li SY, Zhang YL, Tong XZ, Zhang QF (2013) Assessing heavy metal pollution
764 in the water level fluctuation zone of China's Three Gorges Reservoir using
765 geochemical and soil microbial approaches. Environ Monit Assess 185(1): 231–
766 240
767 Ye C, Li SY, Zhang YL, Zhang QF (2011) Assessing soil heavy metal pollution in the
768 water-level-fluctuation zone of the Three Gorges Reservoir, China. J Hazard Mater
769 191(1–3): 366–372
770 Zhang AY, Cornwell W, Li ZJ, Xiong GM, Yang D, Xie ZQ (2019) Dam effect on soil

771 nutrients and potentially toxic metals in a reservoir riparian zone. Clean-Soil Air
772 Water 47(1): 1700497
773 Zhang J, Liu CL (2002) Riverine composition and estuarine geochemistry of particulate
774 metals in China-weathering features, anthropogenic impact and chemical fluxes.
775 Estuar Coast Shelf S 54: 1051–1070
776 Zhang M, Wang XP, Liu C, Lu JY, Qin YH, Mo YK, Xiao PJ, Liu Y (2020)
777 Identification of the heavy metal pollution sources in the rhizosphere soil of
778 farmland irrigated by the Yellow River using PMF analysis combined with
779 multiple analysis methods-using Zhongwei city, Ningxia, as an example. Environ
780 Sci Pollut R 27(14): 16203–16214
781 Zhao LY, Gong DD, Zhao WH, Lin L, Yang WJ, Guo WJ, Tang XQ, Li QY (2020)
782 Spatial-temporal distribution characteristics and health risk assessment of heavy
783 metals in surface water of the Three Gorges Reservoir, China. Sci Total Environ
784 704: 134883
785 Zhou F, Guo HC, Liu L (2007) Quantitative identification and source apportionment of
786 anthropogenic heavy metals in marine sediment of Hong Kong. Environ Geol
787 53(2): 295−305
788 Zhu H, Bing HJ, Wu YH, Zhou J, Sun HY, Wang JP, Wang XX (2019) The spatial and
789 vertical distribution of heavy metal contamination in sediments of the Three
790 Gorges Reservoir determined by anti-seasonal flow regulation. Sci Total Environ
791 664: 79–88
792 Zupancic N, Miler M, Asler A, Pompe N, Jarc S (2021) Contamination of children’s

793 sandboxes with potentially toxic elements in historically polluted industrial city. J
794 Hazard Mater 412: 125275

Table 1 Sediment parameters in the water-level-fluctuation zone of the Three Gorges Reservoir, China.

	pH	OM (mg/g)	TOC (mg/g)	Clay (%)	Silt (%)	Sand (%)	pH	OM (mg/g)	TOC (mg/g)	Clay (%)	Silt (%)	Sand (%)
	(a) After submergence						**(b) Before submergence**					
JJ	7.78	45.53	19.90	1.04	36.30	62.66	7.89	47.28	8.92	0.48	30.82	68.71
XP	7.29	46.75	27.12	0.93	36.82	62.25	7.32	40.74	14.92	1.48	59.68	38.84
BB	7.45	53.87	27.11	0.85	19.31	79.84	7.54	28.12	14.74	0.35	10.10	89.55
TJX	7.48	31.80	19.29	0.36	14.30	85.34	7.88	30.68	10.48	0.64	29.80	69.57
CTM	7.81	35.27	30.97	0.54	24.79	74.67	7.44	33.48	11.03	0.05	1.89	98.06
JGS	7.76	30.45	38.37	1.81	43.63	54.56	7.33	26.76	15.44	0.56	20.46	78.99
TJT	7.88	33.96	23.72	1.66	53.19	45.16	7.87	24.88	8.15	0.40	20.51	79.09
YZ	7.79	24.80	27.91	0.49	13.88	85.64	7.59	45.50	10.51	0.32	12.59	87.09
CS	7.51	40.25	50.09	0.73	22.90	76.37	7.57	25.86	14.18	0.51	21.04	78.46
FL	7.45	30.13	37.65	0.60	21.20	78.20	7.44	57.78	9.78	0.22	8.04	91.74
FD	7.48	35.46	18.21	0.55	14.78	84.67	7.52	39.24	11.74	0.23	5.43	94.34
ZX	7.51	34.36	22.00	0.98	18.14	80.88	7.65	29.86	10.86	0.09	3.80	96.11
WZ	7.78	20.33	21.49	1.77	43.67	54.56	7.76	40.90	11.21	0.08	2.46	97.47
YY	7.29	37.24	31.12	0.30	5.39	94.32	7.49	15.32	9.78	0.08	2.06	97.87
WS	7.88	44.24	21.85	0.37	6.45	93.18	7.81	51.14	8.45	0.09	1.29	98.62
ZG	7.81	20.12	20.59	0.48	24.92	74.61	7.78	45.54	10.26	0.19	6.82	92.99

798 **Table 2** Mean trace metal concentrations in the Three Gorges Reservoir and a comparison with other studies and guidelines (mg·kg^{-1}).

Region	Mn	Fe	V	Cr	As	Ni	Cu	Zn	Sr	Y	Zr	Ba	Pb	Reference
Soils in the TGR														
Agricultural Soil (2013.03)	-	-	-	66	-	8.5	52.2	149	-	-	-	-	13	Liu et al. 2015
Typical agricultural soil in WLFZ[1]	-	-	-	81.5	7.4	31.5	-	71.6	-	-	-	-	25.3	Cheng et al. 2017
Soil (2017.07)	-	-	-	112.9	-	-	53.8	117.3	-	-	-	-	37.3	Zhang et al. 2019
Sediments in the TGR														
Background values	482	27300	76.4	78.0	5.4	29.5	25.0	67.7	121	21.8	237	450	23.9	Wei et al. 1991; Tang et al. 2008
WLFZ [2] (2008.10)	-	-	-	42.0	22.2	-	29.8	76.6	-	-	-	-	35.4	Ye et al. 2011
WLFZ [1] (2009.03)	-	-	-	44.7	6.6	-	35.7	88.1	-	-	-	-	42.9	Ye et al. 2011
WLFZ [2] (2009.06-2009.09)	390.0	24205.0	-	41.2	3.6	-	27.0	75.4	-	-	-	-	32.4	Ye et al. 2013
Xiangxi River (2017.11)	763.6	-	-	56.5	-	17.4	34.6	96.3	-	-	-	655.3	-	Xiong et al. 2020
Main stream of the entire TGR[1] (2018.03)	885.9	39406.3	81.2	77.9	10.3	30.8	41.5	150.3	165.8	34.3	599.8	462.4	45.0	This study
Main stream of the entire TGR[2] (2018.09)	792.0	35118.8	72.4	67.2	8.6	28.2	34.7	121.5	170.3	31.8	582.4	439.7	36.2	This study
Sediments in Other Reservoirs														
Manwan dam in Lancang River, China[1]	-	-	-	44.2	47.8	-	48.5	175.2	-	-	-	-	67.8	Li et al. 2019
Manwan dam in Lancang River, China[2]	-	-	-	55.3	42.3	-	42.4	164.6	-	-	-	-	51.5	Li et al. 2019
Klingenberg Reservoir, Germany	630.0	30700.0		23.1	99.5	23.5		431.0					134.0	Hahn et al. 2019
El Guájaro Reservoir, Colombia	-	-	-	-	-	-	-	-	-	-	78.7	-	5.5	Ana et al. 2018
Sulejów Reservoir, Poland[1]	-	-	-	16.5	-	-	-	-	-	-	-	-	13.6	Aleksandra et al. 2020
Asaker of Aswan High Dam, South Africa[1]	225.5	26575.0	-	11.8	-	45.0	46.5	68.7	-	-	-	-	8.0	Farhat et al. 2018
Hoedong Reservoir, Korea	-	-	-	28.7	-	17.2	56.7	247.8	-	-	-	-	60.5	Lee et al. 2017
Keban Dam Reservoir, Turkey	588.3	61697.7	-	143.6	15.0	106.6	34.5	76.7	-	-	-	-	10.6	Varol 2020
Bontanga Reservoir, Ghana	11.7	262.8	-	0.6	-	-	0.1	0.1	-	-	-	-	-	Asare et al. 2018

799 [1]: after submergence; [2]: before submergence

800

801 **Table 3** Source contribution (%) of sediment metals in study area using positive matrix factorization (PMF) method.

(a) After submergence						**(b) Before submergence**					
Parameters	Ore mining	Domestic sewage	Industrial emissions	Agricultural activities	Natural sources	**Parameters**	Ore mining	Domestic sewage	Industrial emissions	Agricultural activities	Natural sources
Mn	4.8	31.9	9.6	29.3	24.4	Mn	26.5	13.4	25.6	20.2	14.2
Fe	1.8	25.2	30.4	15.2	27.4	Fe	21.1	12.5	23.2	18.9	24.3
V	2.8	25.7	29.1	12.0	30.3	V	19.6	19.4	23.0	12.2	25.9
Cr	0.0	9.2	46.7	5.4	38.7	Cr	17.3	11.2	20.6	22.3	28.6
Ni	0.3	27.2	30.1	14.3	28.1	Ni	18.9	17.6	21.2	16.1	26.3
Cu	5.4	18.8	31.1	43.5	1.2	Cu	11.7	0.0	34.2	40.1	14.0
Zn	31.8	4.3	12.3	25.8	25.8	Zn	38.3	8.3	14.0	39.3	0.1
As	5.0	33.9	8.3	25.9	26.8	As	25.5	43.1	15.1	0.0	16.2
Pb	4.8	18.6	22.4	51.9	2.3	Pb	14.3	0.4	29.2	49.9	6.2

802

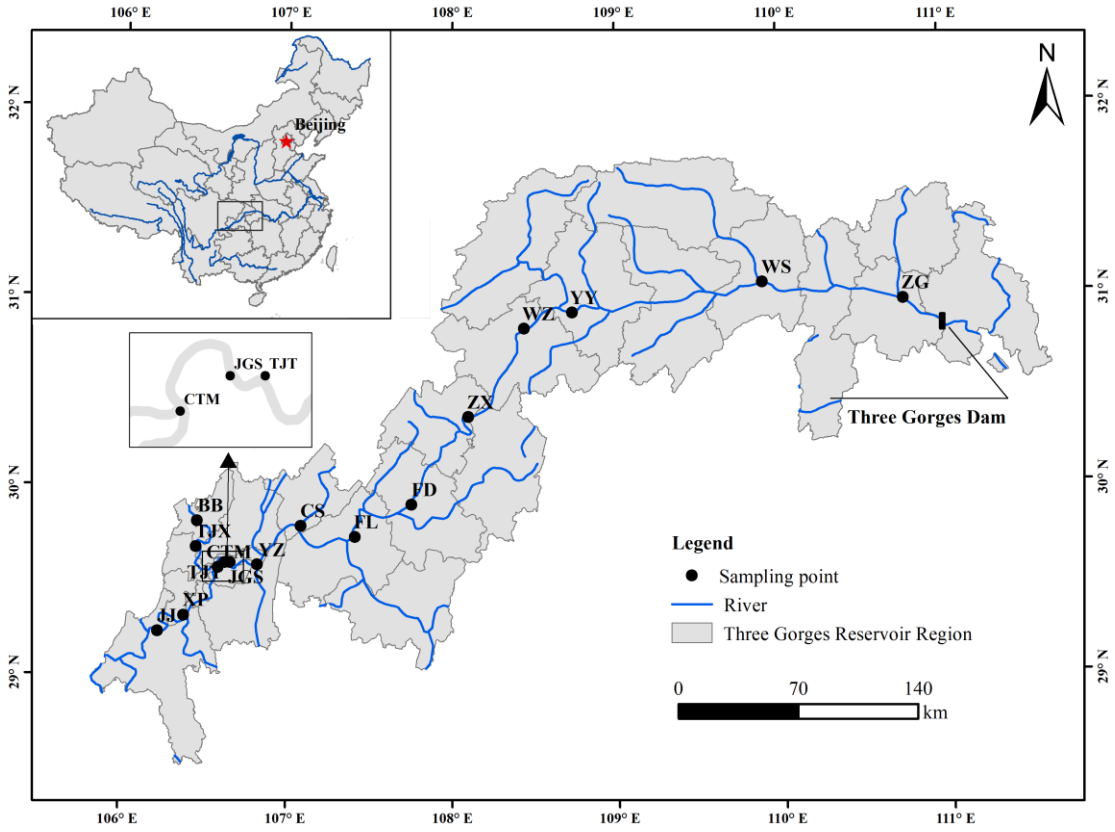

803

804 **Fig. 1** Location of the sampling sites in the water-level-fluctuation zone of Three

805 Gorges Reservoir (TGR).

806

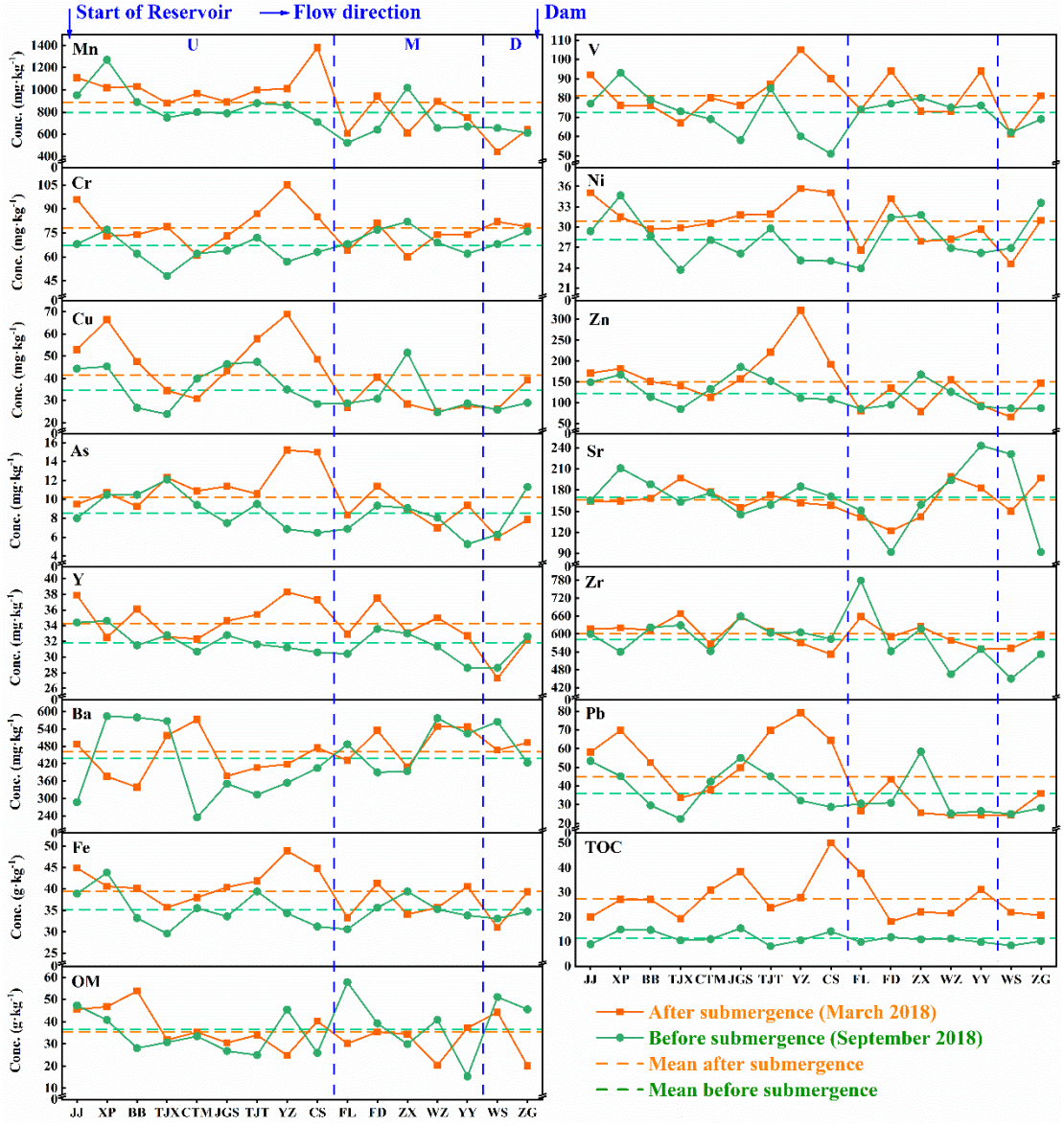

807

808 **Fig. 2** The spatial and temporal distribution of 13 metals, total organic carbon (TOC)

809 and soil organic matter (OM) in the WLFZ of the TGR. *("U" means upstream in TGR; "M"*

810 *means midstream in TGR; "D" means downstream in TGR.)*

811

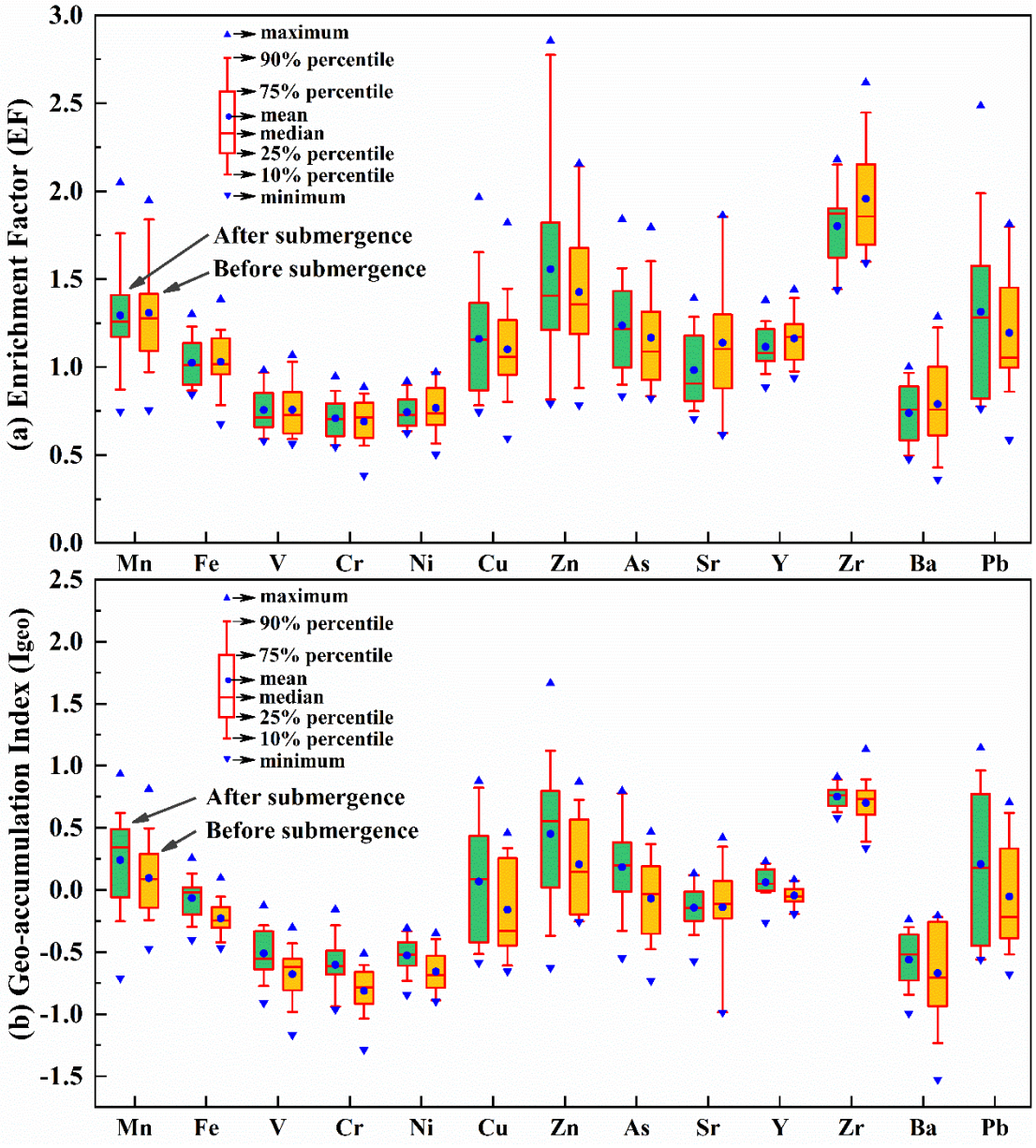

812

813 **Fig. 3** Box plots of enrichment factors (EFs) and the geo-accumulation indices (Igeo)

814 of metals in the WLFZ of the TGR.

815

816

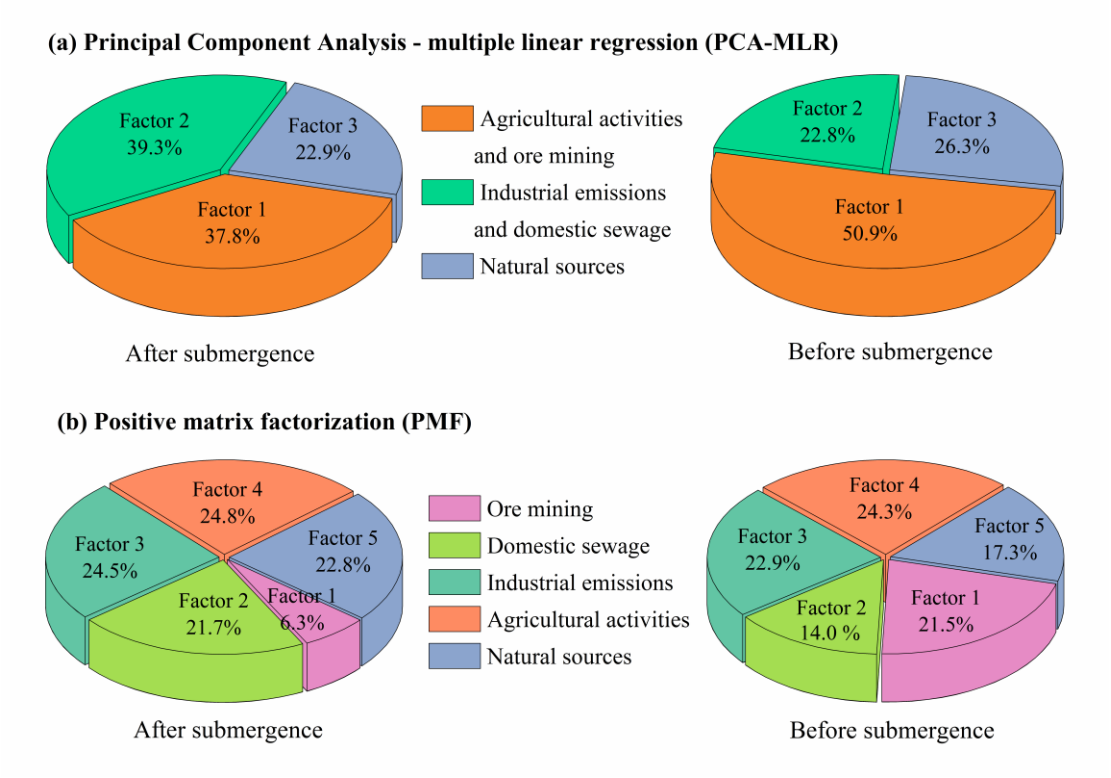

817

818 **Fig. 4** Contribution rates of different sources for metals in the TGR by PCA-MLR and

819 PMF methods.

820

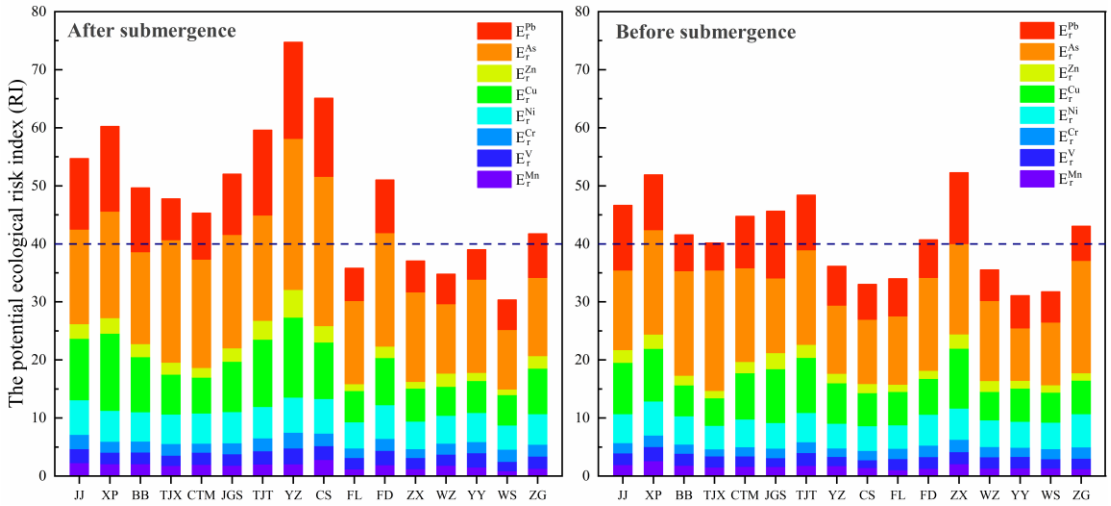

821

822 **Fig. 5** The spatial distribution of the potential ecological risk of trace metals in WLFZ

823 of the TGR.

824

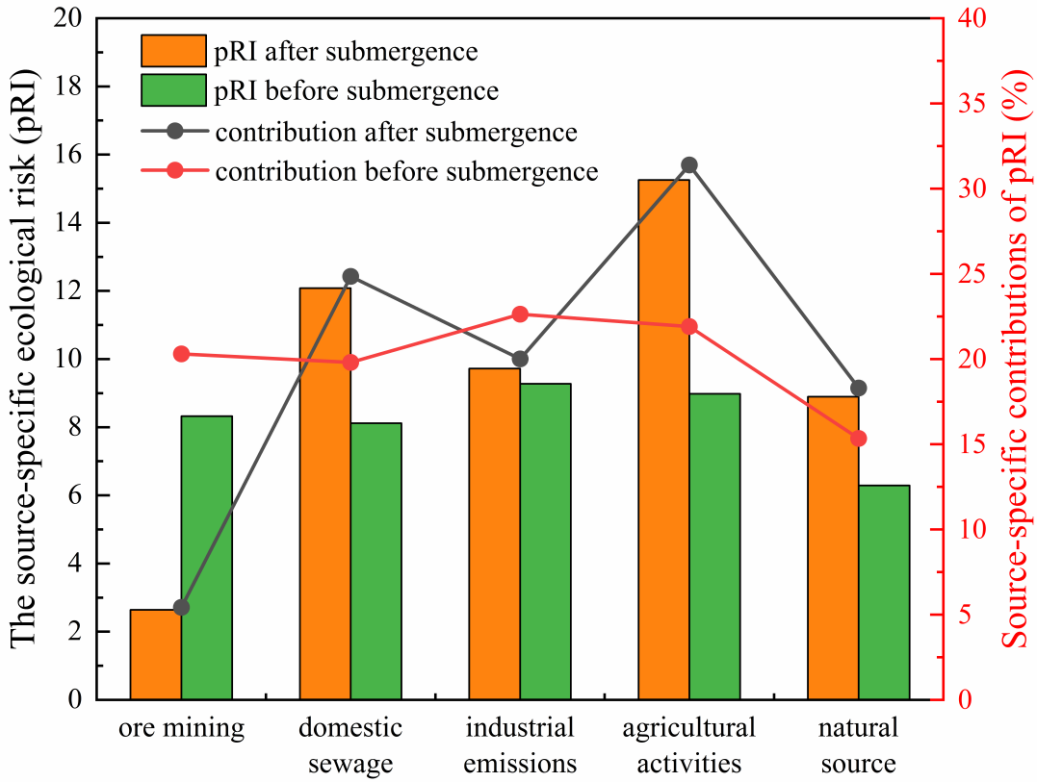

825

826 **Fig. 6** The source-specific ecological risk (pRI) and its corresponding contribution of

827 trace metals in WLFZ of the TGR.

828